ELSEVIER

Journal of Luminescence 62 (1994) 281–289

JOURNAL OF LUMINESCENCE

Optical spectroscopy properties of $BaLiF_3$ doped with Ni^{2+}

E. Martins[a], N.D. Vieira Jr.[a,*], S.L. Baldochi[a], S.P. Morato[a], J.Y. Gesland[b]

[a]*Supervisão de Materiais Optoeletrônicos, Instituto de Pesquisas Energéticas e Nucleares, CP 11.049, CEP 05422-970, São Paulo, SP, Brazil*

[b]*Laboratoire de Physique de L'Etat Condensé, E.R.A. 682, Faculté des Sciences, Route de Laval, 72017 Le Mans Cedex, France*

Received 11 February 1993; revised 25 May 1994; accepted 13 June 1994

Abstract

The basic optical properties of a new perovskite crystal, $BaLiF_3$, doped with Ni^{2+} are reported. We have identified several absorption bands belonging to the Ni^{2+} in an octahedral site by the direct absorption spectrum as well as by the excitation spectrum. The main absorption band peaks at 1180 nm with a $\Delta E/E \approx 30\%$, showing very well defined sharp lines, at low temperature, due to spin–orbit splitting of the excited state. By pumping in any of the absorption bands, a strong emission band peaking at 1.5 μm ($\Delta E/E \approx 20\%$) is observed, with a decay time at room temperature of 3 ms. Besides the 1.5 μm emission band, two other bands were observed, peaking at 480 and 740 nm. All the observed energy transitions are in good agreement with the Tanabe–Sugano model and the measured cross-sections are in the range of the expected ones for allowed magnetic dipole transitions.

1. Introduction

The interest in tunable solid-state lasers has grown by the development of sources based on transitions that are broadened by strong electron–phonon coupling, present in color centers and transition metal ions in solid hosts. The properties of transition metal ions in insulating matrices have received renewed interest since the discovery of the alexandrite laser [1] based on transitions occurring in Cr^{3+} and, recently, in $Ti:Al_2O_3$ [2], among others. The progress made in the understanding of the basic optical spectroscopic properties of similar systems [3] provided the basis for technological achievements in the laser field, with new systems covering the near infrared spectral region [4]. In particular, host materials doped with Ni^{2+} in octahedral sites show a broad vibronically allowed emission band in the near infrared which is useful for tunable solid state lasers in this important spectral region. Although Ni^{2+} in this symmetry has been investigated since 1963 [5], CW laser operation at room temperature has not yet been achieved; the highest operating temperature reported so far is $-30°C$ [3], for the $MgO:Ni^{2+}$ system. Due to strong crystal field dependence of the energy levels of these transition metal ions, the spectroscopic studies of these ions in new hosts are of particular interest. The basic optical spectroscopic properties of Ni^{2+} in a new host, the perovskite $BaLiF_3$, will be described.

*Corresponding author.

SSDI 0022-2313(94)00039-F

2. Experimental

The $BaLiF_3$ crystals doped with Ni^{2+} were grown by the Czochralski technique. The same procedure described was used to grow lead–barium–lithium fluoride [6] and good optical quality, single crystals were obtained ($60\,mm \times \phi \sim 25\,mm$). The Ni concentration actually incorporated in the crystals used was determined by an analytical spectrographic method [7] and the values were between 2.35×10^{19} and 3.91×10^{21} Ni/cm^3. One of the crystals (the one with the lower concentration) was also doped with Pb, in order to reduce oxygen contamination [8]. No significant differences concerning the optical properties of the Ni^{2+} were seen in comparison with the lead undoped ones. Samples were sawed and finely polished for the spectroscopic studies.

The optical absorption spectra were all recorded using a Cary Varian spectrophotometer (model 17D). For the low temperature measurements the sample was placed in a closed-cycle helium cryostat (Displex CS-202, Air Products).

The emission measurements were performed by pumping the crystal with a Nd:YAG laser (model 116, Quantronix) operating at 1.064 μm. The luminescence was collected at 90° and analyzed by a monochromator (model 1870, Spex: 0.5 m, grating 600 g/mm). Detection was done with a cooled InSb detector (mode J10D, EG&G Judson Infrared Inc.) and a lock-in amplifier (model 5209, EG&G Princeton Applied Research). A Kr^+ ion laser (model 400-K3, Coherent Inc.) and an Ar^+ ion laser (model 171-Spectra Physics) were also used as excitation sources. The decay time (τ) measurements were made by a mechanical modulation of the exciting beam, in such way that the on–off time of the laser light was 16 μs. The fluorescence lifetime measurements were done using a fast response germanium detector (EG&G Judson Infrared, Inc., J16, response time 10 μs) and the signals were analyzed by a sampling technique using a boxcar averager (model 4420, EG&G Princeton Applied Research). A 1/4 m monochromator (Jarrell–Ash) was used to analyze the emission spectrum.

The excitation spectrum was obtained using an arrangement of two monochromators. One 1/4 m long (Jarrell–Ash) monochromator to scan the excitation radiation wavelength and one Kratos monochromator to select the emission wavelength. The light source used was a 150 W high pressure xenon lamp, whose intensity was modulated by a chopper (model SR540, Stanford Research Systems, Inc.). An InSb detector operating at 77 K connected to a lock-in amplifier was used for these measurements.

3. Crystal structure

The fluoroperovskite type materials, described by the general formula AMF_3 (A and M mono and divalent cations, respectively), crystallize in a single cubic system; they belong to the space group O_h^1 or P_{m3m}, as shown in Fig. 1. The crystalline structure

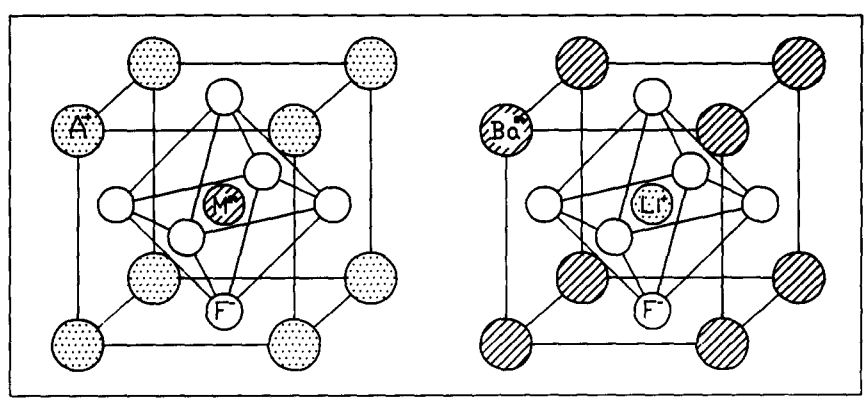

Fig. 1. Crystalline structure of the fluoroperovskite AMF_3 (left side) and the $BaLiF_3$ crystal (right side).

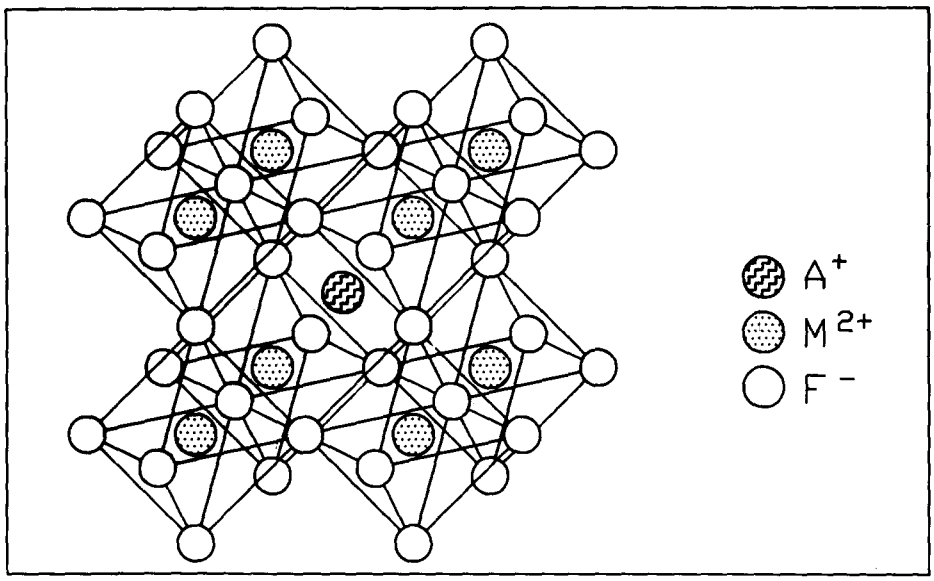

Fig. 2. Diagram of the piling of the MF_6 octahedra for the fluoroperovskite structure.

can be described as a piling of MF_6 arranged in the form of tridimensional octahedra as shown in Fig. 2. $BaLiF_3$ is an inverted perovskite compared to the classical perovskite (Fig. 1), where Barium and Lithium are in exchanged positions [Ba (1/2, 1/2, 1/2) and Li (0, 0, 0)]. In spite of this fact, the local symmetry is the same (O_h) [9].

The pure $BaLiF_3$ material is a colorless crystal, transparent from UV (140 nm) up to IR (6 μm) (band gap = 8.7 eV) [10], presenting a refraction index of 1.544 at 589 nm, a lattice parameter of 3.995 Å and a density of 5.243 g/cm^3 [11]. The crystal is nonhygroscopic, showing a high chemical stability and does not show phase transitions in the range of temperature used in our experiments. They present visual transparency, free from evident inhomogeneities and none of them cracked even without an annealing treatment after crystal growth.

4. Results and discussion

4.1. Absorption spectra

The room temperature absorption spectrum of $BaLiF_3:Ni^{2+}$ for the sample of 2.5 mol% Ni concentration and 7.8 mm thick is shown in Fig. 3. The general structure of the spectrum is quite similar to the $KMgF_3:Ni^{2+}$ and $KNiF_3$ [12] ones, and it is clearly seen three main, broad, absorption bands peaking at 1180, 700 and 390 nm. Besides, there is a small band peaking at about 645 nm, that overlaps the 700 nm band. As shown by fitting the bands with gaussian shapes, there is a structureless weaker broad absorption band peaking at 450 nm. These absorption bands were labeled in terms of the crystal field splitting of the d orbitals and the electron–electron interaction of the ion Ni^{2+} in an octahedral environment, according to the classical Tanabe–Sugano diagram [13]. The most intense bands correspond to electronic transitions between the ground state, $^3A_{2g}$, and three other states of symmetries $^3T_{2g}$, $^3T^a_{1g}$, and $^3T^b_{1g}$, respectively.

The absorption spectrum of the lower concentration sample (0.15 mol%), 5.4 mm thick, at 10 K, is shown in Fig. 4. The main characteristics of the room temperature bands remain, with the exception of the presence of narrow, no-phonon lines (detail in Fig. 4). Following the same arguments given in Ref. [14], we attribute to the character of the 1180 nm band ($^3A_{2g} \rightarrow {}^3T_{2g}$) of magnetic dipole. The sharp no-phonon lines indicate the pure

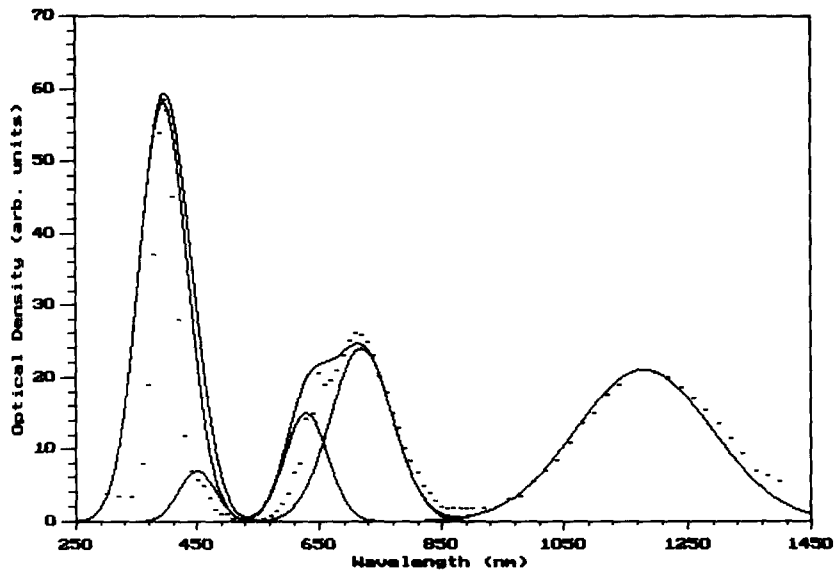

Fig. 3. Room temperature optical absorption spectrum of the $BaLiF_3:Ni^{2+}$ crystal, with a Gaussian fit.

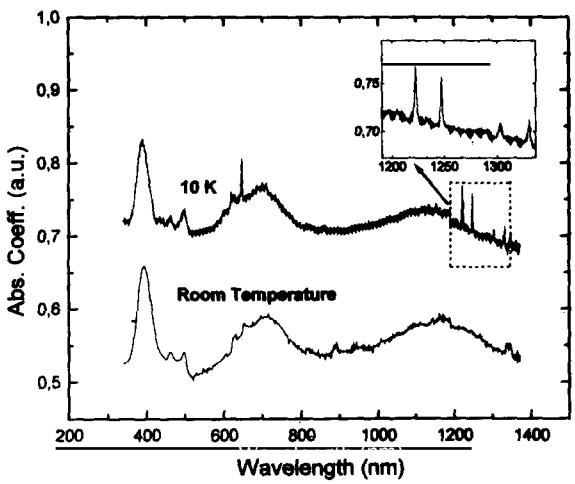

Fig. 4. Absorption spectrum of the lower concentration $BaLiF_3:Ni^{2+}$ crystal at room temperature and 10 K. The sharp lines are shown in detail.

electric transitions to the spin–orbit components of the $^3T_{2g}$ level.

There are four sharp lines in the long wavelength side of the 1180 nm. The 1222 nm (8183.3 cm^{-1}, full width at half maximum (FWHM) $\approx$ 2.6 cm^{-1}), the 1247 nm (8019.3 cm^{-1}, FWHM $\approx$ 3.5 cm^{-1}), the 1302 nm (7680.5 cm^{-1}, FWHM $\approx$ 5.0 cm^{-1}) and the 1330 nm (7518.8 cm^{-1} FWHM $\approx$ 3.0 cm^{-1}), which are interpreted [15], respectively, as transitions to the Γ_2, Γ_5, Γ_4, Γ_3 spin–orbit components of the $^3T_{2g}$ state. The spin–orbit splitting between the 1222 nm and the 1247 lines is 164 cm^{-1} and between the 1302 nm and the 1330 lines is 161.7 cm^{-1}. They are closely related to the $KMgF_3:Ni^{2+}$ and $KZnF_3:Ni^{2+}$ systems, that have a spin–orbit splitting of the same order [16].

As can be clearly seen in Fig. 4, the increase of temperature to 300 K does not change significantly the total oscillator strength of this band, with the exception of the disappearance of the sharp lines. Therefore we conclude that, even at room temperature, phonon assisted electric dipole transitions are not significant for the fundamental absorption band.

In particular, the bands overlapping the short wavelength side of the 700 nm band appear as a structured sequence of narrow lines over a broad band at the pedestal. Among those, there is one that appears (broadened) also at room temperature (645 nm) and does not change significantly the peak wavelength with temperature variation, corresponding to the transition from ground state $^3A_{2g}$ to

^1E_g excited state. The band shape does not change significantly up to 100 K, temperature in which the sharp lines of the other bands have disappeared. Notice the high intensity of this band, that is due to a strong mixing with the close-lying spin allowed $^3T^a_{1g}$ band and very weak electron–phonon interaction. This is one of basis of the energy levels assignment. The assignment was completed by taking the ratio of the main transitions, 1180, 700, 645, 450 and 390 nm, from the ground state $^3A_{2g}$ to the excited states $^3T_{2g}$, $^3T^a_{1g}$, ^1E_g, $^1T_{2g}$ and $^3T^b_{1g}$, respectively. In order to obtain the crystal field parameter corresponding to the energy splitting of the d orbitals in a cubic symmetry, we applied the theoretical model of Liehr and Ballhausen [17]. For simplicity we take the maxima of the bands at room temperature. The best fit corresponds to a crystal field parameter $Dq/B = 0.88$. The cubic field schemes of Tanabe–Sugano [13] and of Liehr and Ballhausen [17] are very convenient for an overall calculation of the energy levels for similar compounds. The crystalline-field parameter Dq is greater than in the other Ni doped fluoroperovskites [12], as the unit cell is smaller (lattice parameter $a_0 = 4.014$ Å in $KNiF_3$, $a_0 = 4.00$ Å in $KMgF_3$:Ni^{2+} and $a_0 = 3.995$ Å in $BaLiF_3$:Ni^{2+}). Table 1 shows the transitions energies and the corresponding level assignment.

The band peaking at 390 nm ($^3A_{2g} \rightarrow {}^3T^b_{1g}$) is the most intense transition seen in these spectral range. It is much narrower, the shape is temperature independent and there is no clear evidence of sharp structure. Similarly to the $KMgF_3$:Ni^{2+} [15], we attribute the width to the small spin–orbit splitting of the $^3T^b_{1g}$ level.

We have observed that, besides the characteristic absorptions of Ni^{2+} in octahedral sites, there is an unknown absorption in the UV region (200 nm). This band does not change peak position with concentration, and will be subject of further investigations.

In the lower Ni concentration sample this UV band has the peak position shifted to 240 nm. By chemical analysis, a significant Pb concentration was determined in this sample (1.5×10^{19} Pb/cm^3), and this UV band is probably due to Pb ions aggregated with Ni ions, since Pb in $BaLiF_3$ does not show any absorption in the 240 nm region [18].

Table 1
Observed energies of Ni^{2+} in $BaLiF_3$

Transition	Energy [cm^{-1}]
$^3A_{2g} \rightarrow {}^3T_{2g}$	8695.65
$^3A_{2g} \rightarrow {}^3T^a_{1g}$	14285.71
$^3A_{2g} \rightarrow {}^1E_g$	15503.88
$^3A_{2g} \rightarrow {}^1T_{2g}$	22222.22
$^3A_{2g} \rightarrow {}^3T^b_{1g}$	25641.03

Table 2
Absorption cross-section [$\times 10^{-20}$ cm^2]

Band peak [nm]	Room temperature	Band peak [nm]	10 K
390	4.37	380	4.80
700	3.41	690	3.15
1180	2.87	1150	2.96

The absorption cross-section (σ_a) was calculated from the absorption coefficient ($\alpha_a\,\text{cm}^{-1} = \sigma_a\,[\text{Ni}]$) and the measured Ni concentration, ([Ni]). Table 2 shows the absorption cross-sections as function of temperature for the sample of 0.15 mol% Ni concentration.

4.2. Luminescence

As in other Ni^{2+} doped fluoroperovskites ($KZnF_3$ and $KMgF_3$) [19], three bands belonging to this ion in an octahedral site are observed in the luminescence spectra of the $BaLiF_3$:Ni^{2+}, two in the near infrared and one in the green region. The 1.5 μm infrared emission can be conveniently pumped in the 1180 nm absorption band (with the 1.064 μm Nd:YAG laser line, at room temperature) and is shown in Fig. 5. It appears as an intense broad band ($\Delta\nu = 4 \times 10^{13}$ Hz) peaking at 1.5 μm, corresponding the transition between the lowest excited state manifold, $^3T_{2g}$ and the ground state $^3A_{2g}$. This emission was also observed by pumping in the any of the others absorption bands, indicating that either by a relaxation process or emission process the $^3T_{2g}$ energy level is populated. Preliminar results show that the low temperature

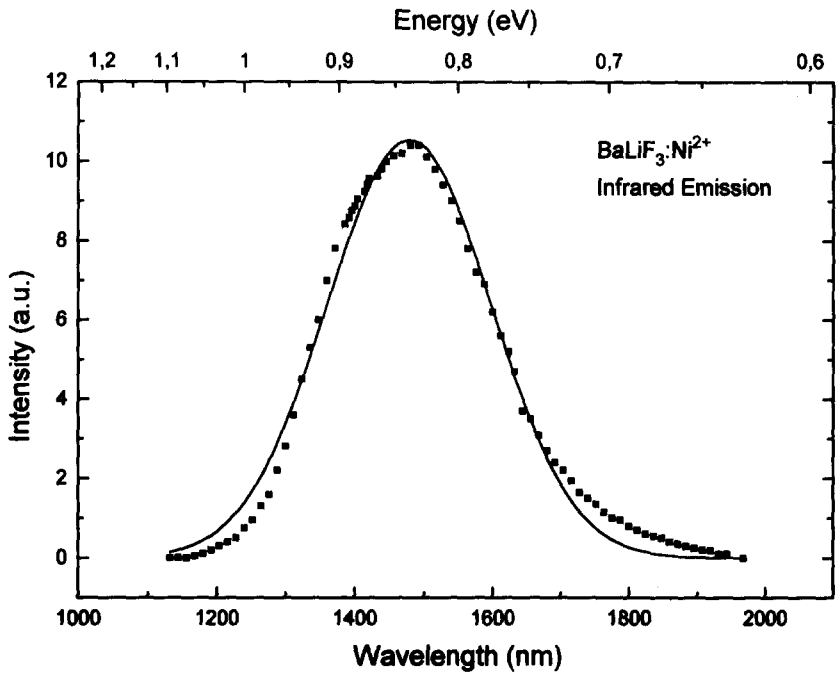

Fig. 5. Infrared emission spectrum of the $BaLiF_3:Ni^{2+}$ at room temperature. The solid line is the Gaussian fit to the data. The excitation wavelength is 1.064 μm Nd:YAG laser line.

emission spectrum is very structured, presenting several sharp lines besides the no-phonon lines mentioned in Section 4.1, and will be subject of further investigation.

By pumping either the $^3T^b_{1g}$ state or $^1T_{2g}$ states we can observe the emission bands in green region and near infrared region (the called "red emission" for other perovskites crystals) [20].

The red band, peaking at 740 nm, is observed by pumping the $^1T_{2g}$ absorption band peaking at 450 nm by the Ar^+ ion laser line (457.9 nm) and is shown in Fig. 6. The green emission, peaking at 480 nm, can be observed in the spectrum of Fig. 7, at room temperature. It was observed using a Xe arc lamp as a pumping source at 390 nm or exciting the crystal with an Ar^+ ion laser operating in the ultraviolet region (multi-line; 351.1–363.8 nm). Therefore, we conclude that the two higher energy emissions derive from the $^1T_{2g}$ level. Furthermore, the more energetic band (480 nm) results from a transition which terminates on the ground state ($^3A_{2g}$), while the lower energy transition (740 nm) terminate on the first excited level ($^3T_{2g}$). The sum of the transition energies $[(1500\text{ nm})^{-1} + (740\text{ nm})^{-1}]$ is almost exactly the energy of the more energetic transition $(480\text{ nm})^{-1}$. These measured results were also seen by Vehse et al. [19] in other perovskites materials. The green emission band ($^1T_{2g} \rightarrow {}^3A_{2g}$) does not significantly change its shape and magnitude and it shows, as well as the absorption band at 390 nm, a much narrower bandwidth. The intensity of the 480 nm band is several orders higher (ten times) than the 740 nm emission.

4.3. Luminescence decay time

The intensity temporal behavior of the 1.5 μm luminescence band was detected, stored and displayed by a boxcar averager. Fig. 8 shows the temporal behavior of luminescence signal; it shows a single exponential decay with a time constant of $\tau = 3 \pm 0.2$ ms, at room temperature. By pumping the crystal with a Kr^+ ion laser operating at

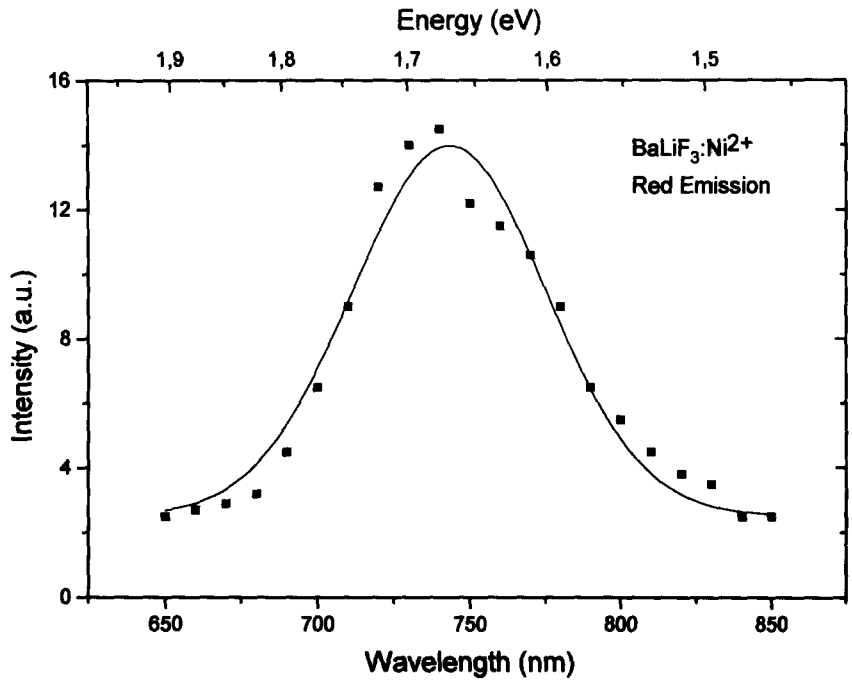

Fig. 6. Red emission band peaking at 740 nm of the $BaLiF_3:Ni^{2+}$, at room temperature, by pumping with the Ar ion laser line (457.9 nm), with a Gaussian fit to the data.

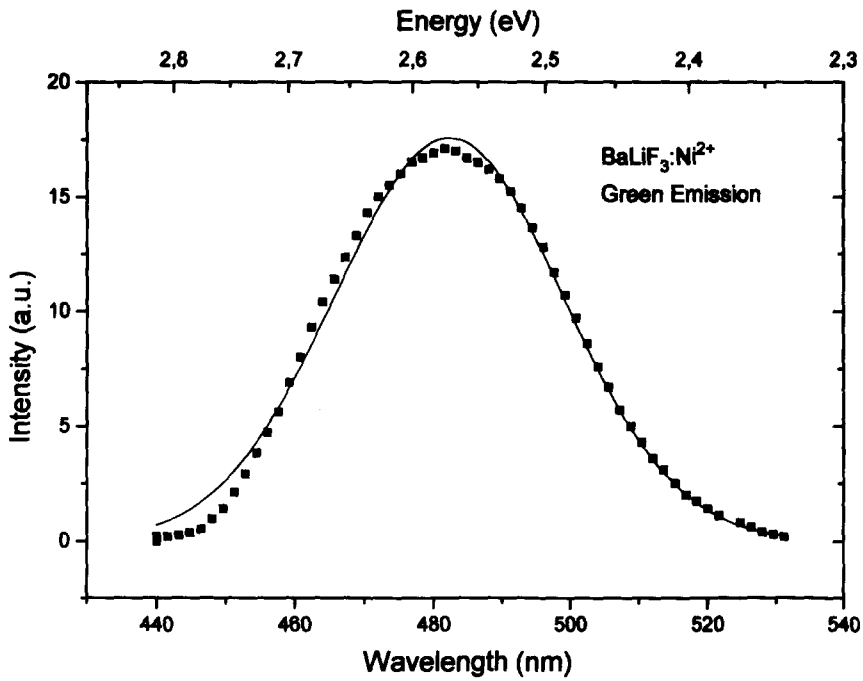

Fig. 7. Green emission of the $BaLiF_3:Ni^{2+}$ when pumping in the UV region, at room temperature, with a Gaussian fit to the data.

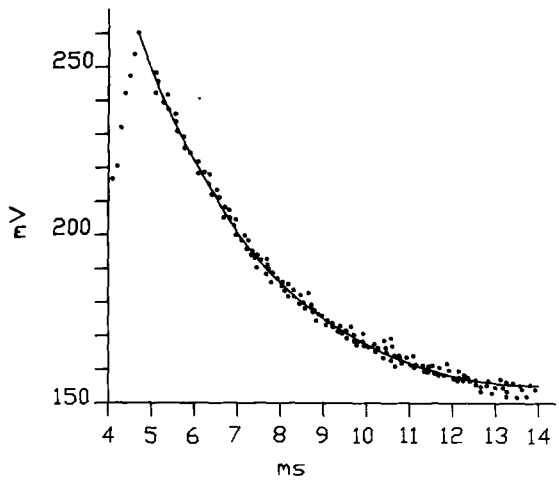

Fig. 8. Temporal behavior of the luminescence intensity when excited by a modulated 1064 nm beam. The solid line is the fit of an exponential decay with a constant of 3 ms (0.2 ms).

647 nm, (that overlaps very well with the 700 nm band) the same decay time, for the 1.5 μm band, was measured. Considering that τ is the luminescence decay time (i.e., the quantum efficiency is unity), we can determine [21] the oscillator strength, f_{lum}, from formula (1):

$$f_{lum} = \frac{\lambda^2}{8\pi^2 cnr_0 \tau \left[\frac{(n^2+2)}{3}\right]^2}, \quad (1)$$

where c is the speed of the light in vacuum, r_0 the classical electron radius, λ the vacuum wavelength and n the index of refraction of the host. For $\tau = 3$ ms, $\lambda = 1.5$ μm and $n = 1.544$, expression (1) yields a very modest oscillator strength, $f_{lum} = 0.362 \times 10^{-6}$. It must be stressed that this value is the uppermost limit since we have not studied the temperature and concentration behavior of this crystal.

The estimated maximum peak emission cross section can also be calculated [21] by the expression (2):

$$\sigma = \frac{2}{\Delta\nu}\left[\frac{\ln 2}{\pi}\right]^{1/2} \frac{\lambda^2}{8\pi^2 \tau n^2}, \quad (2)$$

where $\Delta\nu$ is the full width at half maximum of the emission. The emission cross section is 3×10^{-21} cm^2 at the peak of the band (1.5 μm). Note that this result is based on the assumption that the quantum efficiency is unity. For practical laser developments this is a bottleneck that will impose crystals with high concentrations to provide a significant small signal gain coefficient.

4.4. Excitation spectrum

The Ni^{2+} bands that appeared in the absorption spectrum (Fig. 3), are also identified by the excitation spectrum, as shown in Fig. 9. To obtain the excitation spectrum, the peak of broad band fluorescence (centered at 1.5 μm) was used as the monitoring wavelength. Due to the limited range of the monochromator, the infrared region was not studied, but, as shown before, the main absorption band peaking at 1180 nm is the fundamental transition that gives rise to the 1.5 μm emission band.

5. Conclusion

The optical absorption spectrum shown in Fig. 3 is characteristic of Ni^{2+} in an octahedral environment. In particular very similar spectra have been reported for $KNiF_3$ and $KMgF_3$:Ni^{2+} [12,15]. Using the simplified Tanabe and Sugano energy level diagram [13], we could determine the normalization constant B (the Racah parameter) and the crystal field parameter (Dq), by the peak positions of the transitions between the fundamental state $^3A_{2g}$ and the excited states $^3T_{2g}$ and $^3T_{1g}$, respectively. The resulting fitting parameters for the $BaLiF_3$:Ni^{2+} crystal are $Dq = 847.5$ cm^{-1} and $B = 957.7$ cm^{-1} ($Dq/B = 0.88$). As in the case of $KZnF_3$, $KMgF_3$ and $KNiF_3$ ($Dq = 725$ cm^{-1}) [14], the $BaLiF_3$ lattice is in the intermediary crystal field region, that allows for vibronic lower lying transitions.

One very interesting fact is that the absorption peak cross sections do not vary significantly with temperature, indicating that the nature of the transition is predominantly of magnetic dipole character, as seen in other systems (MgO, MgF_2 and $KMgF_3$). By measuring the concentration of Ni^{2+} in $BaLiF_3$ we could determine the absorption cross section of all the observed bands, that are in

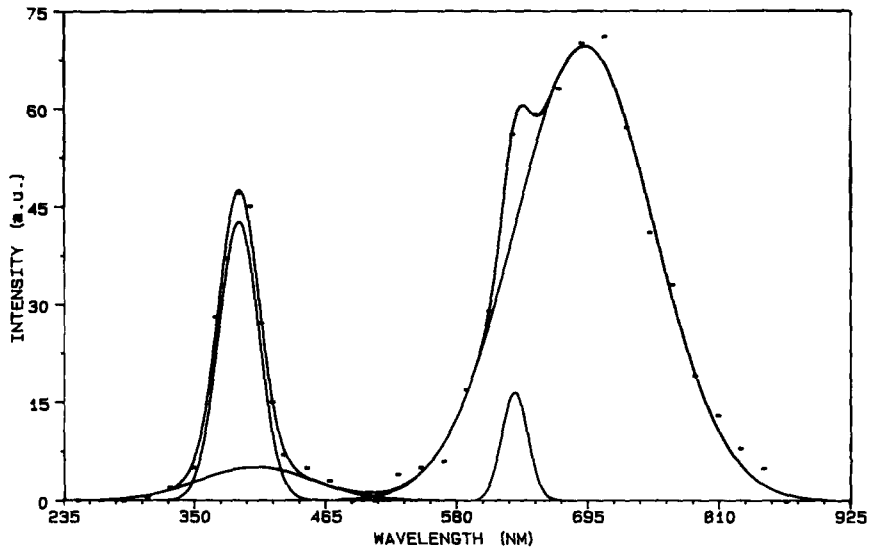

Fig. 9. Excitation spectrum of the $BaLiF_3:Ni^{2+}$ at 10 K, with the monitoring wavelength at 1.5 μm (dots). The solid line is the fit using gaussian profiles for the several absorption bands. The peaks of the bands are 390, 645 and 700 nm.

the order of 10^{-20} cm^2. This fact, together with the long decay time measurement of the main emission is consistent with the above statement of the magnetic dipole character of the transitions.

Summarizing, the $BaLiF_3:Ni^{2+}$ shows very interesting properties: the host shows good optical properties, the absorption of the main transition band overlaps the strong Nd laser emission line and the emission covers the region around 1.5 μm. There are several points that must still be investigated, such as the dependence on Ni concentration in this crystal, the cooperative effects at high concentrations and, mostly, excited state absorption. This is crucial to the operation of this new laser candidate.

References

[1] J.C. Walling, O.G. Peterson, H.P. Jenssen, R.C. Morris, E.W. O'Dell, IEEE J. Quantum Electron. QE-16 (1980) 1302.
[2] J. Harrison, Proc. OSA Tech. Digest, Advanced Solid State Lasers Conference, Hilton Head, NC, 1991.
[3] P.F. Moulton, A. Mooradian, T.B. Freed, Opt. Lett. 3 (1978) 164; also in P.F. Moulton, A. Mooradian, Appl. Phys. Lett. 35 (1979) 838.
[4] P.F. Moulton, IEEE J. Quantum Electron. QE-21 (1985) 1582.
[5] L.F. Johnson, R.E. Deitz, H.J. Guggenheim, Phys. Rev. Lett. 11 (1963) 318.
[6] S.L. Baldochi, J.Y. Gesland, Mat. Res. Bull. 27 (1992) 891.
[7] S.F. Sabato, IPEN/CNEN Internal Publication (1989) QI-012.
[8] R.C. Pastor, A.C. Pastor, Mat. Res. Bull. 10 (1975) 117.
[9] F.S. Galassso, in: Structure and Properties of Inorganic Solids (Pergamon Press, 1970).
[10] N. Kristianpoller, A. Rehavi, B. Trieman, Ann. Isr. Phys. Soc. 6 (1984) 395.
[11] K. Recker, F. Wallrafen, K. Dupré, Naturwissenschaft 75 (1988) 156.
[12] K. Knox, R.G. Shulman, S. Sugano, Phys. Rev. 130(2) (1963) 512.
[13] Y. Tanabe, S. Sugano, J. Phys. Soc. Jpn. 9 (1954) 753; also in S. Sugano, Y. Tanabe, H. Kamimura, in: Multiplets of Transition Metal Ions in Crystals (Academic Press, New York, London, 1970).
[14] J. Ferguson, H.J. Guggenheim, L.F. Johnson, H. Kamimura, J. Chem. Phys. 38 (1963) 2579.
[15] J. Ferguson, H.J. Guggenhein, D.L. Wood, J. Chem. Phys. 40 (1964) 822.
[16] J. Ferguson, H.J. Guggenhein, J. Chem. Phys. 44 (1966) 1095.
[17] A.D. Liehr, C.J. Ballhausen, Ann. Phys. 6 (1959) 134.
[18] L. Prado, N.D. Vieira, S.L. Baldochi, S.P. Morato, J.Y. Gesland, Solid State Commun. 87 (1993) 41.
[19] W.E. Vehse, K.H. Lee, S.I. Yun, W.A. Sibley, J. Lumin. 10 (1975) 149.
[20] M.V. Iverson, W.A. Sibley, J. Lumin. 20 (1979) 311.
[21] B. Di Bartolo, in: Optical Interactions in Solids (Wiley, 1968).